BJP BRITISH JOURNAL OF PHARMACOLOGY
BPS BRITISH PHARMACOLOGICAL SOCIETY

BJP British Journal of Pharmacology

DOI:10.1111/j.1476-5381.2010.00886.x
www.brjpharmacol.org

RESEARCH PAPER

Pentobarbital inhibition of human recombinant α_{1A} P/Q-type voltage-gated calcium channels involves slow, open channel block

A Schober, E Sokolova and KJ Gingrich

The Department of Anesthesiology, New York University Langone Medical Center, New York, USA

Correspondence
Kevin J. Gingrich, Department of Anesthesiology, NYU Langone Medical Center, 550 1st Avenue RR-605, New York, New York 10016, USA. E-mail: kevin.gingrich@nyumc.org

Keywords
P/Q Ca^{+2} channels; $Ca_V2.1$; pentobarbital; electrophysiology; pharmacology; recombinant proteins

Received
24 December 2009
Revised
25 February 2010
Accepted
11 April 2010

BACKGROUND AND PURPOSE

Pre-synaptic neurotransmitter release is largely dependent on Ca^{2+} entry through P/Q-type ($Ca_V2.1$) voltage-gated Ca^{2+} channels (PQCCs) at most mammalian, central, fast synapses. Barbiturates are clinical depressants and inhibit pre-synaptic Ca^{2+} entry. PQCC barbiturate pharmacology is generally unclear, specifically in man. The pharmacology of the barbiturate pentobarbital (PB) in human recombinant α_{1A} PQCCs has been characterized.

EXPERIMENTAL APPROACH

PB effects on macroscopic Ca^{2+}(I_{Ca}) and Ba^{2+}(I_{Ba}) currents were studied using whole-cell patch clamp recording in HEK-293 cells heterologously expressing $(\alpha_{1A})_{human}(\beta_{2a}\alpha_2\delta\text{-}1)_{rabbit}$ PQCCs.

KEY RESULTS

PB reversibly depressed peak current (I_{peak}) and enhanced apparent inactivation (fractional current at 800 ms, r_{800}) in a concentration-dependent fashion irrespective of charge carrier (50% inhibitory concentration: I_{peak}, 656 μM; r_{800}, 104 μM). Rate of mono-exponential I_{Ba} decay was linearly dependent on PB concentration. PB reduced channel availability by deepening non-steady-state inactivation curves without altering voltage dependence, slowed recovery from activity-induced unavailable states and produced use-dependent block. PB (100 μM) induced use-dependent block during physiological, high frequency pulse trains and overall depressed PQCC activity by two-fold.

CONCLUSION AND IMPLICATIONS

The results support a PB pharmacological mechanism involving a modulated receptor with preferential slow, bimolecular, open channel block (K_d = 15 μM). Clinical PB concentrations (<200 μM) inhibit PQCC during high frequency activation that reduces computed neurotransmitter release by 16-fold and is comparable to the magnitude of Ca^{2+}-dependent facilitation, G-protein modulation and intrinsic inactivation that play critical roles in PQCC modulation underlying synaptic plasticity. The results are consistent with the hypothesis that PB inhibition of PQCCs contributes to central nervous system depression underlying anticonvulsant therapy and general anaesthesia.

Abbreviations

CDI, Ca^{2+}-dependent inactivation; PB, pentobarbital; PQCC, P/Q-type voltage-gated Ca^{2+} channel; VACC, voltage-activated Ca^{2+} current; VDI, voltage-dependent inactivation

Introduction

Voltage-activated Ca^{2+} currents (VACC) have diverse physiological and pharmacological properties and have been classified into five broad categories (L-, P/Q-, N-, R- and T-type) based on features of activation, inactivation and susceptibility to peptide blockers. The associated channel proteins have been identified and labelled using the Ca_Vx nomenclature (Catterall *et al.*, 2003). These channels are expressed

as a membrane complex consisting of a primary α_1 pore-forming subunit accompanied by β, $\alpha_2\delta$ and γ accessory subunits. Expression of the α_1 subunit alone is sufficient to form a functional channel, but the presence of β and $\alpha_2\delta$ subunits are required for normal channel expression and gating properties. Ca^{2+} entry through P/Q-type ($Ca_V2.1$) voltage-gated Ca^{2+} channels (PQCC) is a dominant trigger for neurotransmission at most fast conventional synapses in the mammalian central nervous system (CNS), and are integral components of the pre-synaptic neurotransmitter release machinery. In addition, pre-synaptic neurotransmitter release is proportional to up to the 4th power of Ca^{2+} entry. Therefore, PQCCs represent a high gain system for the regulation of synaptic transmission in the CNS in which small fractional changes in Ca^{2+} entry through these channels may profoundly affect neuronal signalling (for reviews, see Catterall, 2000; Catterall and Few, 2008).

Barbiturates depress the CNS providing for clinical utility as general anaesthetics and anticonvulsants. CNS depression arises from their well-known enhancement of inhibitory post-synaptic Cl^- currents carried by $GABA_A$ receptors (Evans, 1979; Mathers and Barker, 1980; Olsen, 1988; Macdonald *et al*. 1989), and also by inhibition of excitatory pre-synaptic neurotransmitter release (Brooks and Eckert, 1947; Weakly, 1969; Richards, 1972; Baudoux *et al*., 2003) involving reduced Ca^{2+} entry into the pre-synaptic nerve terminal (Morgan and Bryant, 1977; Leslie *et al*. 1980; Baudoux *et al*., 2003). Therefore, inhibition of pre-synaptic PQCCs may contribute to CNS depression produced by barbiturates. The barbiturate pentobarbital (PB) inhibits excitatory neurotransmitter release in brain slices by a mechanism involving alterations in PQCC function (Kitayama *et al*., 2002). Previous investigations have generally reported that PB enhances apparent inactivation of N-, L-type or mixed populations of neuronal VACCs (Nishi and Oyama, 1983; Ikemoto *et al*. 1986; Gross and Macdonald, 1988; Gundersen *et al*., 1988;ffrench-Mullen *et al*., 1993) leading to the proposal that PB and other barbiturates modulate voltage-dependent inactivation (VDI) (Nishi and Oyama, 1983; Ikemoto *et al*. 1986; Gross and Macdonald, 1988; Gundersen *et al*., 1988). PB also inhibits rat, reticular thalamocortical, T-type currents and those of recombinant $Ca_V3.3$ (Joksovic *et al*., 2005), $Ca_V3.1$ and $Ca_V3.2$ channels (Todorovic *et al*., 2000). There is only a single investigation, to our knowledge, that selectively examined PB modulation of PQCCs, as assayed by changes in infrequent peak I_{Ba}s, which reported little depression at clinically relevant concentrations (Hall *et al*., 1994). Overall, the pharmacological mechanism governing PB modulation of PQCCs remains unknown, as well as its possible role in CNS depression. Finally, it is important to examine PB pharmacology in human PQCCs since PB anaesthetic potency appears to be species dependent (Spector, 1956; Richards, 1972; Franks and Lieb, 1993).

To address these questions, we investigated the inhibitory effects of PB on human recombinant α_{1A} PQCCs heterologously expressed in HEK-293 cells, which manifest inactivation and facilitation that closely resembles the behaviour of pre-synaptic PQCCs recorded from the Calyx of Held synapse in the rat brainstem (Lee *et al*., 2000). This approach provides a homogeneous channel population, avoids the uncontrollable complexities of the synaptic milieu and provides for the study of a human α_{1A} subunit in a heterologous channel. We studied the $(\alpha_{1A})_{human}(\beta_{2a}\alpha_2\delta\text{-}1)_{rabbit}$ channel complex which probably reflects the function of the human channel since the primary α_{1A} isoform is derived from man (Soong *et al*., 2002) and the α subunit includes the conduction pore, voltage sensors and most of the binding sites for second messengers, drugs and toxins (Catterall, 2000). We included the β_{2a} subtype to facilitate investigation of PB effects on inactivation since it produces slow inactivation allowing resolution of changes in current time course, simplifies the inactivation mechanism by precluding preferential closed-state inactivation (Patil *et al*., 1998; Lee *et al*. 2000) and also results in a channel complex prevalent in many regions of the brain (Stea *et al*., 1994; Tanaka *et al*. 1995). PQCCs manifest calcium-dependent inactivation (CDI) that is triggered by elevated global cytosolic Ca^2 and which can only be observed under experimental conditions that employ near-physiological cytosolic Ca^{2+} concentrations (Lee *et al*., 2000; Liang *et al*. 2003). Therefore, to investigate the effects of PB on CDI, we used mild Ca^{2+} buffering in whole-cell, patch-clamp, pipette solutions, which produces near-physiological cytosolic Ca^{2+} concentrations (Lee *et al*., 2000; Liang *et al*. 2003).

Methods

The nomenclature used conforms to the *British Journal of Pharmacology*'s 'Guide to Receptors and Channels' (Alexander *et al*., 2008).

Cell culture and transient transfection

Transformed HEK-293 cells, purchased from American Type Culture Collection (Bethesda, MD, USA), were plated on 12 × 12 mm glass coverslips in 60 × 15 mm Falcon dishes (Becton Dickinson, Lincoln

Park, NJ, USA) and cultured in minimum essential medium (MEM) supplemented with 10% fetal bovine serum and penicillin (100 IU·mL^{-1}), streptomycin (0.1 mg·mL^{-1}) and glutamine (2 mM) all from Invitrogen (Carlsbad, CA, USA). After incubation in 37°C, 5% CO2 for 48 h, cells were transiently transfected using a lipofection technique described previously (Gingrich *et al.*, 2009) with cDNAs encoding wild-type human α_{1A} pore-forming subunit (Soong *et al.*, 2002), rabbit β_{2a} (Perez-Reyes *et al.*, 1992) and rabbit skeletal muscle $\alpha_2\delta$-1 (Tomlinson *et al.*, 1993) accessory subunits and the respiratory syncytial virus T antigen. The β_{2a} subunit also encoded a green fluorescent protein (GFP) sequence following an internal ribosomal entry site, so as to identify successfully transfected HEK-293 cells by fluorescence (Chaudhuri *et al.*, 2007). Briefly, aliquots of lipofection reagent (Lipofectamine, Life Technologies, Carlsbad, CA, USA) and appropriate plasmids (1:1:1:0.5 by weight, $\alpha_{1A}/\beta_{2a}/\alpha_2\delta$-1/T antigen) were mixed in a modified, serum-free medium (Optimem, Invitrogen), and incubated at room temperature for 10 min. Cells were washed with PBS (Invitrogen), and supplemented MEM was replaced with Optimem, followed by addition of liposome-plasmid containing solution. After a 3–4 h incubation period (37°C, 5% CO2), cells were washed with PBS and returned to supplemented MEM for further incubation. Cells were ready for electrophysiological recording 48 h after transfection.

Electrophysiology

Whole-cell barium (I_{Ba}) and calcium (I_{Ca}) currents were recorded at room temperature 48–96 h post-transfection from individual cells presumably co-expressing β_{2a} and GFP as identified by fluorescence microscopy. Both Ba^{2+} and Ca^{2+} were used as charge carriers in order to differentiate between effects on VDI and CDI. Cells were voltage clamped using the whole-cell configuration of the patch-clamp technique at room temperature. Data were collected using an Axopatch 200A amplifier (Axon Instruments, Union City, CA, USA) connected to an IBM-compatible computer running the Matlab (Mathworks, Natick, MA, USA) environment and software of our own design.

Extracellular solutions contained 130 mM N-methyl-D-glucamine, 130 mM aspartic acid, 1 mM $MgCl_2$-H_2O, 10 mM glucose, 10 mM 4-aminopyridine, 10 mM HEPES, 10 mM $BaCl_2$ or $CaCl_2$, pH 7.3–7.4 with aspartic acid. Internal solutions contained 135 mM caesium methansulphonate, 5 mM CsCl, 1 mM $MgCl_2$, 4 mM Mg-adenosine triphosphate, 5 mM HEPES and 0.5 mM EGTA, pH 7.3–7.4 with CsOH. Buffering with 0.5 mM EGTA provided near-physiological internal calcium buffering (free $[Ca^{2+}] \cong 100$ nM). Currents were sampled at 10 kHz and filtered at 2 kHz. Currents were measured (–90 mV holding potential, HP) in control and in the presence of PB (0–500 μM). Leak and capacitive transients were subtracted using a P/8 protocol. Cells were continuously superfused with solutions delivered by a dual-barreled, local solution changer, which involved a closed system constructed entirely of stainless steel, glass, polytetrafluoroethylene tubing and glass syringes with a syringe pump. This system provides complete cell bathing solution changes within 2 s.

By using the internal and external solutions described, pipette resistances were 2–5 MΩ, which were series compensated by greater than 60%. The barbiturate PB (Sigma-Aldrich, St. Louis, MO, USA) was diluted from a 5 mM stock solution on the day of experimentation and was loaded into the local solution changer. Current–voltage (*I–V*) relationships in control solution were obtained at the beginning and end of each experimental period. Results obtained from cells with outward currents or atypical *I–V* relationships at either time point were discarded. Currents were obtained in control, drug, wash sequence unless otherwise stated and data were included only when the measures of current amplitude and inactivation in the wash response were within 10% of initial control. These stringent inclusion criteria were necessary to ensure a stable preparation required for detailed time course analysis. As a result, data were collected from less than 5% of cells that were successfully voltage clamped, which typically showed recording stability for <30 min. Cells appeared to poorly tolerate the near-physiological cytosolic Ca^{2+} concentrations obtained from mild buffering conditions, which probably contributed to the difficulty in obtaining long periods of preparation stability. Experiments involving voltage protocols promoting inactivation were repeated no more frequently than every 60 s to allow for recovery of activity-induced unavailable channels between stimuli in both control and drug (see Figure 6). Therefore, protocols involving a wide range of voltages were collected in two subsets involving depolarizing voltages that were either odd and/or even multiples of 10 mV.

Data analysis

Curve fitting and statistical analysis were performed with ORIGIN software (OriginLab, Northampton, MA, USA). The data are shown as mean ± SEM, unless otherwise stated. Paired and unpaired *t*-tests were applied as appropriate and significance was taken at $P < 0.05$. The maximum channel conductance (G_{peak}) was calculated using $[G = I/(V - V_{rev})]$ where V is the voltage of the activating

depolarization, I is the current maximum during the activating depolarization and V_{rev} is the current reversal potential as estimated by extrapolating the quasi-linear portion of the current–voltage (I–V) relation to zero current at positive voltages. Voltage dependence of activation was quantified by first relating peak G normalized by maximum G to the activating voltage, which was followed by a quantitative description of this relation using a two-state Boltzmann equation of the form [Normalized $G = (1 - P)/\{1 + \exp([V - V_{1/2}]/dx)\} + P$] where V is voltage, $V_{1/2}$ is the midpoint voltage, P is the plateau value, and dx is the slope factor. Concentration–inhibition relations were fit with a logistic equation of the form [$Y = 1/\{1 + IC_{50}/[PB]^{slope}\}$] where Y is the response variable, [PB] is the PB concentration, IC_{50} is the concentration at 50% inhibition from control and *slope* is the factor related to the Hill coefficient. Response time courses were fit with a bi-exponential function [$A_1 \bullet \exp(-t/\tau_1) + A_2 \bullet \exp(-t/\tau_2) + B$] where A_n is the nth component amplitude, B is a constant representing a plateau, t is time and τ_n is the nth component time constant.

Results

PB depressed peak current and enhanced apparent inactivation

We were interested in examining overall PB effects on human α_{1A} PQCCs as well as specifically investigating the role of inactivation in the pharmacological mechanism. PQCCs manifest both VDI and CDI (Catterall and Few, 2008). We began by investigating the PB effects on the current peak and decay triggered by depolarizations long enough (800 ms) to induce both VDI and CDI. Figure 1A (left) shows current responses from an individual cell expressing human PQCCs with Ca^{2+} as the charge carrier (I_{Ca}). Control I_{Ca} activated rapidly, reaching a peak within 50 ms, followed by monotonous decay reflecting both CDI and VDI, which together reduced current by nearly threefold, consistent with previous results (Lee *et al.*, 2000). Fractional current remaining at the end of the 800 ms depolarization (r_{800}) was taken as a measure of inactivation. 50 μM PB depressed peak I_{Ca} and accelerated current decay reflecting enhanced apparent inactivation as quantified by r_{800} depression. A higher PB concentration (500 μM) potentiated both effects (Figure 1A, lower left) indicating concentration dependence. The onset and offset of PB effects occurred within ~50 s given a voltage stimulus period of 60 s, initiation of cell bathing solution exchanges within ~5 s of the preceding voltage stimulus and solution exchange kinetics of ~2 s (Figure 1B, inset). The findings in individual cells were confirmed in concentration–response relationships in grouped data over a range of concentrations (Figure 1B). Inactivation enhancement (r_{800}) was marked over the clinically relevant concentrations (<200 μM). Depression of peak I_{Ca} was less sensitive to PB relative to inactivation as reflected by a 10-fold greater IC_{50} and ~50% shallower slope of the fitted logistic equation. Notably, peak current depression (50 μM) was nearly twofold greater than previously reported in rodent cerebellum (Hall *et al.*, 1994). CDI is triggered by Ca^{2+} binding to calmodulin that is pre-associated with the PQCC complex (Lee *et al.*, 1999; DeMaria *et al.* 2001; Erickson *et al.*, 2001). Therefore, to investigate these effects in the absence of CDI, Ca^{2+} was replaced by Ba^{2+} as the charge carrier since Ba^{2+} poorly activates calmodulin (Chao *et al.*, 1984). In Figure 1A (right), control I_{Ba}s manifests minimal decay indicating near elimination of CDI and demonstrate that PB produced similar effects on I_{Ba} as for I_{Ca}, at both concentrations in individual cells. Concentration–response relationships in grouped data for I_{Ba} were similar to those of I_{Ca}. These findings indicate that Ca^{2+} binding to calmodulin and subsequent CDI play little role in PB action, and point to selective PB enhancement of VDI. PB effects on peak current and inactivation were reversible and data were included only when washout peak

Figure 1

Concentration-dependence of the peak current depression and enhancement of apparent inactivation induced by pentobarbital. (A) Currents triggered by test pulses (protocol above) with $Ca^{2+}(I_{Ca})$ and $Ba^{2+}(I_{Ba})$ as charge carriers in control (CTL) and pentobarbital (PB) at indicated concentrations from individual cells expressing $(\alpha_{1A})_{human}(\beta_{2a}\alpha_2\delta\text{-}1)_{rabbit}$ channels. Depolarization produced downward current deflection marking channel activation, which was followed by current decay reflecting inactivation. Solid horizontal line marks baseline and tail currents were clipped for display purposes. Both 50 μM (above) and 500 μM (below) PB depressed peak current (I_{peak}), accelerated current decay and apparent inactivation (shown by fractional current at 800 ms, r_{800} indicated by horizontal arrow) for both charge carriers. The responses to PB were replotted after normalization to control I_{peak} (norm PB, dotted line) to illustrate potentiated current decay. PB 500 μM panels include a response following ~110 s washout period (Washout, dashed lines) that are representative and which nearly superimpose on baseline control responses, indicating preparation stability and reversibility of PB effects. (B) I_{peak} and r_{800} (fraction of control) concentration–response relationships for both charge carriers (means ± SEM, n = 3–7). Smooth curves are logistic function fits (estimated value ± SE) of grouped I_{peak} (IC_{50} = 656 ± 56 μM, slope = 0.86 ± 0.06) and r_{800} (IC_{50} = 104 μM ±, slope = 1.37 ± 0.08) data (see Methods), see text. Inset shows representative time course of I_{peak} and r_{800}* (current magnitude at the end of the 800 ms pulse) from an individual cell during multiple exposures to 500 μM PB (open horizontal bars).

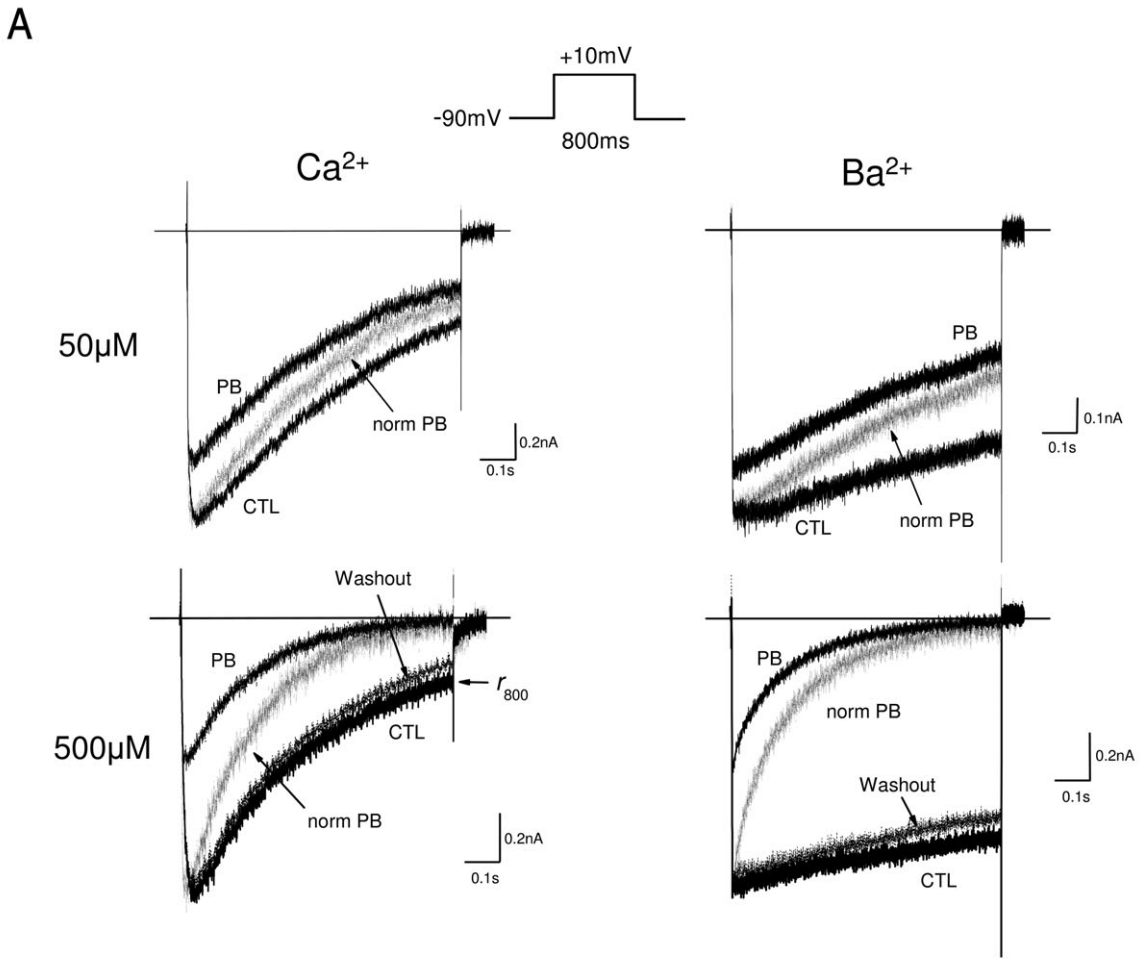
A
+10mV
-90mV
800ms
Ca2+
Ba2+
50μM
PB
norm PB
CTL
0.2nA
0.1s
0.1nA
0.1s
Washout
r800
500μM

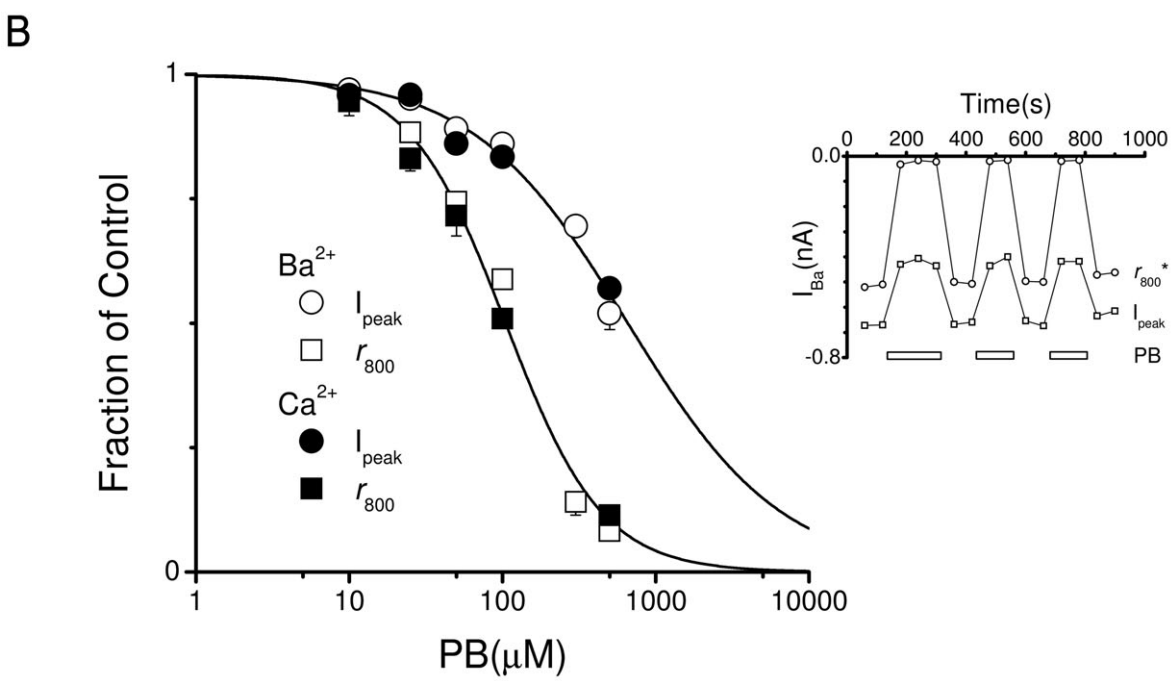
B
Fraction of Control
PB(μM)
Ba2+
Ipeak
r800
Ca2+
Ipeak
r800
Time(s)
IBa(nA)
r800*
Ipeak
PB

current and r_{800} returned to near-baseline control values prior to PB exposure (see Methods). Figure 1A (lower trace) shows representative control/wash pairs for both charge carriers where washout responses nearly superimpose with those of baseline controls. PB is structurally related to the non-anaesthetic barbituric acid, which was employed as a negative control. Barbituric acid (500 μM) failed to significantly alter peak I_{Ba} and r_{800} (normalized to control: peak, 1.02 ± 0.034; r_{800}, 1.01 ± 0.04, compared to unity $P < 0.37$ and 0.39, respectively, $n = 3$, data not shown).

PB-induced inhibition of peak current was independent of activating voltage

PB depression of peak current may be explained by block of resting channels, as well as by alterations in activation or permeation. To address the latter two possibilities, we investigated PB effects on current–voltage (*I*–V) relationships. Figure 2A (upper traces) shows response families from individual cells triggered by 25 ms depolarizations over a range of voltages with Ca^{2+} (left) and Ba^{2+} (right) as charge carriers. I_{Ca} activation time course was slower than that for I_{Ba} consistent with previous results (Chaudhuri *et al.*, 2007). We investigated the effects of 500 μM PB, which is near the IC_{50} for peak current depression, so that its effects could be easily resolved. However, this concentration produced discernible current decay during 25 ms depolarizations (data not shown) that was not present in control with both charge carriers (Figure 2A, upper trace). Therefore, pulse durations were shortened individually for each charge carrier such that current decay during the pulse was no longer appreciable (Figure 2A, lower trace), thereby minimizing potential accumulation of unavailable states during the collection of an *I*–*V* response family. PB appeared to depress peak I_{Ca} and I_{Ba} from individual cells in a uniform fashion over the voltage range tested, which was also evident in *I*–*V* relationships in grouped data (Figure 2B) as reduced amplitude unattended by changes in form. To further explore possible effects on activation, we constructed normalized conductance–voltage (*G*–V) relationships (see Methods). In control, the Ba^{2+} relationship was shifted leftward by ~2 mV relative to that for Ca^{2+} (Figure 2C) similar to previous reports (Lee *et al.*, 1999). *G*–*V* relationships in control and 500 μM PB were similar with both charge carriers, lending further support to minimal PB effects on activation. The results suggest that peak current depression arises from the reduction of channels available for activation at resting membrane potentials, which may occur when resting channels undergo direct blockade or alternatively are promoted to VDI states.

Calcium-dependent facilitation and deactivation were insensitive to PB

PQCCs exhibit Ca^{2+}-dependent facilitation (CDF) in which Ca^{2+} entry during a conditioning prepulse potentiates subsequent activation, which involves Ca^{2+} binding to calmodulin independent of G-protein regulation (Lee *et al.*, 2000; 2003; DeMaria *et al.*, 2001). To investigate possible PB effects on CDF, we studied I_{Ca}s triggered by a test pulse with and without a preceding conditioning pulse using a two-pulse protocol (conditioning pulse, +20 mV, 25 ms; test pulse, +10 mV, 50 ms). Depolarizations were delivered from a HP of –90 mV and conditioning and test pulses were separated by a 10 ms period at HP. A +20 mV conditioning pulse was chosen to induce CDF because it triggers minimal relief of G-protein inhibition (Chaudhuri *et al.*, 2007). In this paradigm, the conditioning pulse accelerated the activation time course of the test pulse I_{Ca}, which represents CDF. To quantify changes in the activation time course, we determined the time from 10 to 90% of peak I_{Ca} ($t_{10–90}$). Without the conditioning pulse, the test pulse triggered slowly activating I_{Ca}s reaching a maximum at pulse end, which is consistent with previous reports (Chaudhuri *et al.*, 2007) and responses obtained in experiments contributing to *I*–*V* relationships (Figure 2A, left upper trace). Conditioning pulse application significantly accelerated the test pulse I_{Ca} activation time course reducing $t_{10–90}$ from 13.4 ± 7.9 ms to 3.53 ± 0.51 ms ($P < 0.05$, $n = 4$, data not shown) consistent with

Figure 2

Effects of pentobarbital on current– and conductance–voltage relationships. (A) I_{Ca} (left) and I_{Ba} (right) families triggered by a range of depolarization voltages (protocols above) in control (CTL, above) and 500 μM pentobarbital (PB, below) from single cells expressing P/Q-type voltage-gated Ca^{2+} channels. Pulse depolarizations shortened in the presence of PB to minimize inactivation, see text. Straight lines mark baselines and tail currents were clipped for clarity. Stimulus period was 15 s. (B) Control current–voltage (*I*–V) relationship plots for normalized peak I_{Ca} (left) and I_{Ba} (right) (means ± SEM, $n = 4–6$). Responses to 500 μM PB normalized by CTL rendered *I*–V relationships that are uniformly attenuated for both charge carriers. (C) Plots of normalized conductances for Ca^{2+} (G_{Ca}, left) and Ba^{2+} (G_{Ba}, right) versus voltage representing activation curves which demonstrate similar relationships for CTL and PB. Curved lines are Boltzmann function fits of control responses (G_{Ca}: $V_{1/2} = –2.4$ mV, slope = 4.7; G_{Ba}: $V_{1/2} = –0.6$ mV, slope = 4.2), see Methods.

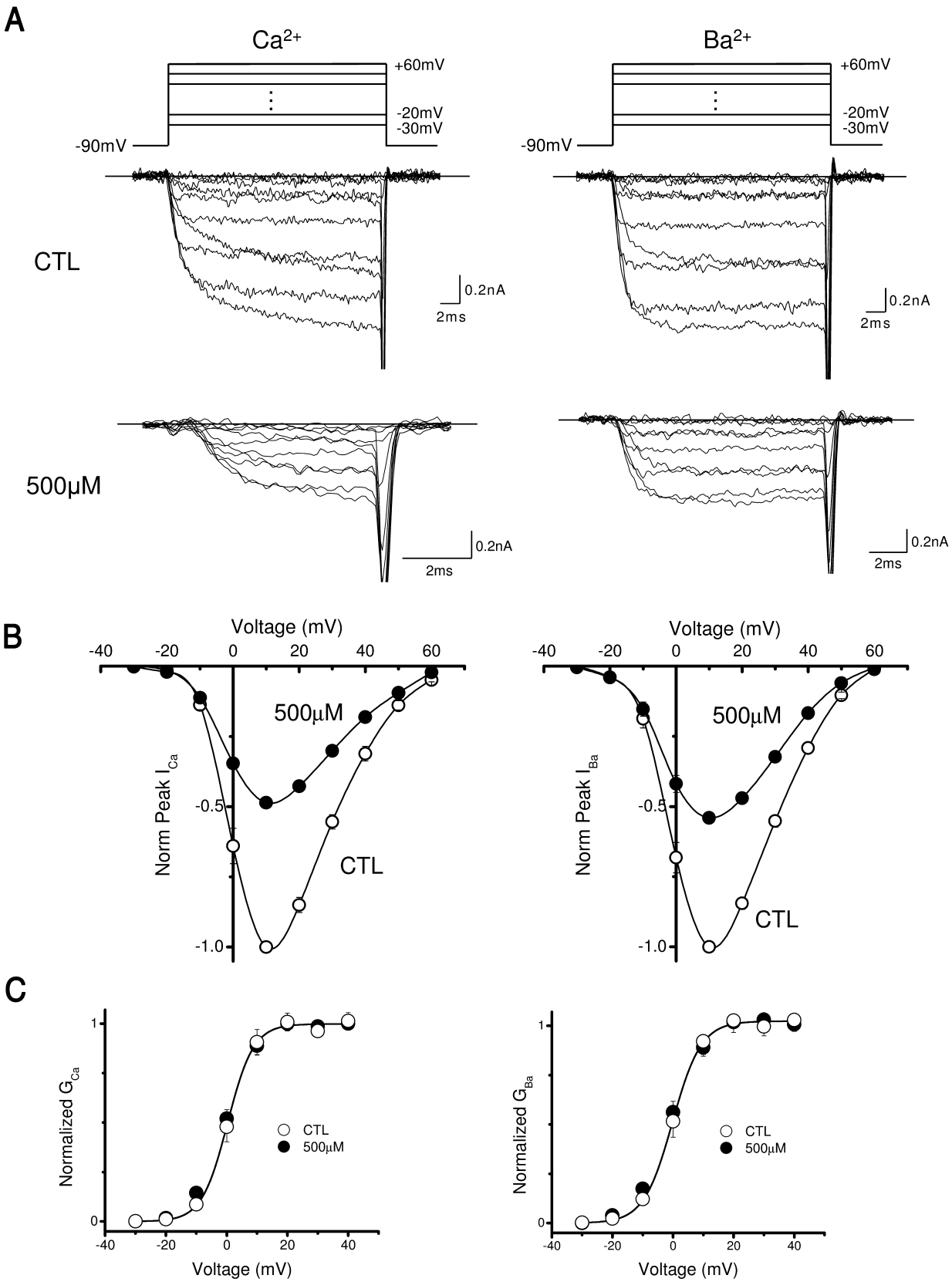
A
Ca2+
Ba2+
+60mV
-20mV
-30mV
-90mV
CTL
500μM
0.2nA
2ms
B
Voltage (mV)
-40
-20
0
20
40
60
500μM
CTL
Norm Peak ICa
Norm Peak IBa
-0.5
-1.0
C
Normalized GCa
Normalized GBa
1
0
CTL
500μM
Voltage (mV)

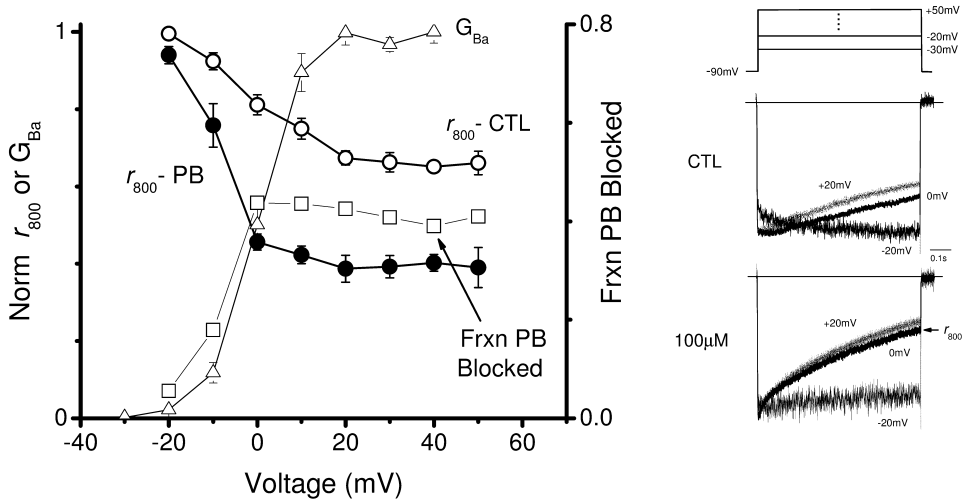

Figure 3

Pentobarbital modulation of apparent voltage-dependent inactivation. Right, selected I_{Ba}s from a cell expressing P/Q-type voltage-gated Ca^{2+} channels triggered by the voltage protocol indicated (above) in control (CTL, middle) and 100 μM pentobarbital (100 μM, below) normalized to peak current to illustrate differences in current time course. Noise appears greater in PB responses due to the greater magnification caused by current reduction by resting block. The current remaining at the end of the 800 ms depolarization (r_{800}) is indicated by the arrow, for the 100 μM PB response triggered by 0 mV. Left, voltage dependence of r_{800} in control (r_{800}-CTL) and 100 μM PB (r_{800}-PB), fraction of inactivated channels blocked by PB (Frxn PB Blocked, complement of r_{800} of 100 μM PB normalized to that of control), and G_{Ba} as replotted from Figure 2C in grouped data (means ± SEM, n = 3–8), see text.

previous reports (Lee *et al.*, 2000; Chaudhuri *et al.* 2007). In the same cells, 100 μM PB depressed the test pulse I_{Ca} independent of the conditioning pre-pulse. The conditioning pre-pulse reduced t_{10-90} from 12.6 ± 6.5 ms to 3.47 ± 0.48 ms (data not shown), which were not significantly different compared to control (P < 0.65 and P < 0.85, respectively, n = 4). To test whether PB affects voltage-mediated closure of activation gates, we investigated deactivation. Tail current deactivation (voltage paradigm of Figure 1A) time course was well fit by a mono-exponential function (not shown) in which associated time constants were unaffected by 100 μM PB (control, 0.29 ± 0.063 ms; PB, 0.3 ± 0.048 ms; P < 0.67, n = 5). The results suggest that PB produces little effect on CDF and deactivation.

PB enhanced apparent VDI

Our results so far show that PB effects are independent of charge carrier, which indicates that mechanisms activated by Ca^{2+} entry are not involved and suggests that PB causes block of resting channels or promotes VDI at resting membrane potentials. We next focused on VDI by employing Ba^{2+} as the charge carrier, which minimizes CDI. We examined PB effects on current decay over a range of activating voltages. Figure 3 (right) shows I_{Ba}s triggered by selected depolarizations from an individual cell in control. Current decay reflecting VDI is absent at a triggering voltage of –20 mV, whereas 0 mV produced marked decay that was enhanced little by increasing the depolarization (+20 mV), demonstrating a plateau effect. Inactivation curves obtained by plotting r_{800} depression versus voltage confirmed these observations in grouped data (Figure 3, left). The control inactivation curve reached a plateau near the peak of the *G–V* relationship (+20 mV) consistent with traditional open channel inactivation (Armstrong and Bezanilla, 1977; Bean, 1981). PB (100 μM) produced little depression of r_{800} at –20 mV in individual responses from the same cell (Figure 3, right). However, r_{800} depression at 0 mV and +20 mV was greater and, to a similar degree, relative to control. These observations indicate PB enhancement is voltage dependent reaching a plateau at depolarizing potentials exceeding 0 mV. The associated inactivation curve in grouped data (Figure 3, left) accords with these observations. The complement of the PB inactivation curve normalized by control yields the fraction of inactivated channels that are blocked by PB (Frxn PB Blocked) versus voltage. This function increases with voltage and reaches a plateau near the maximum of the *G–V* relationship, consistent with PB acting on channel states visited subsequent to activation, which include open, inactivated or nearby states. These observations are consistent with direct PB modulation of VDI or open channel block.

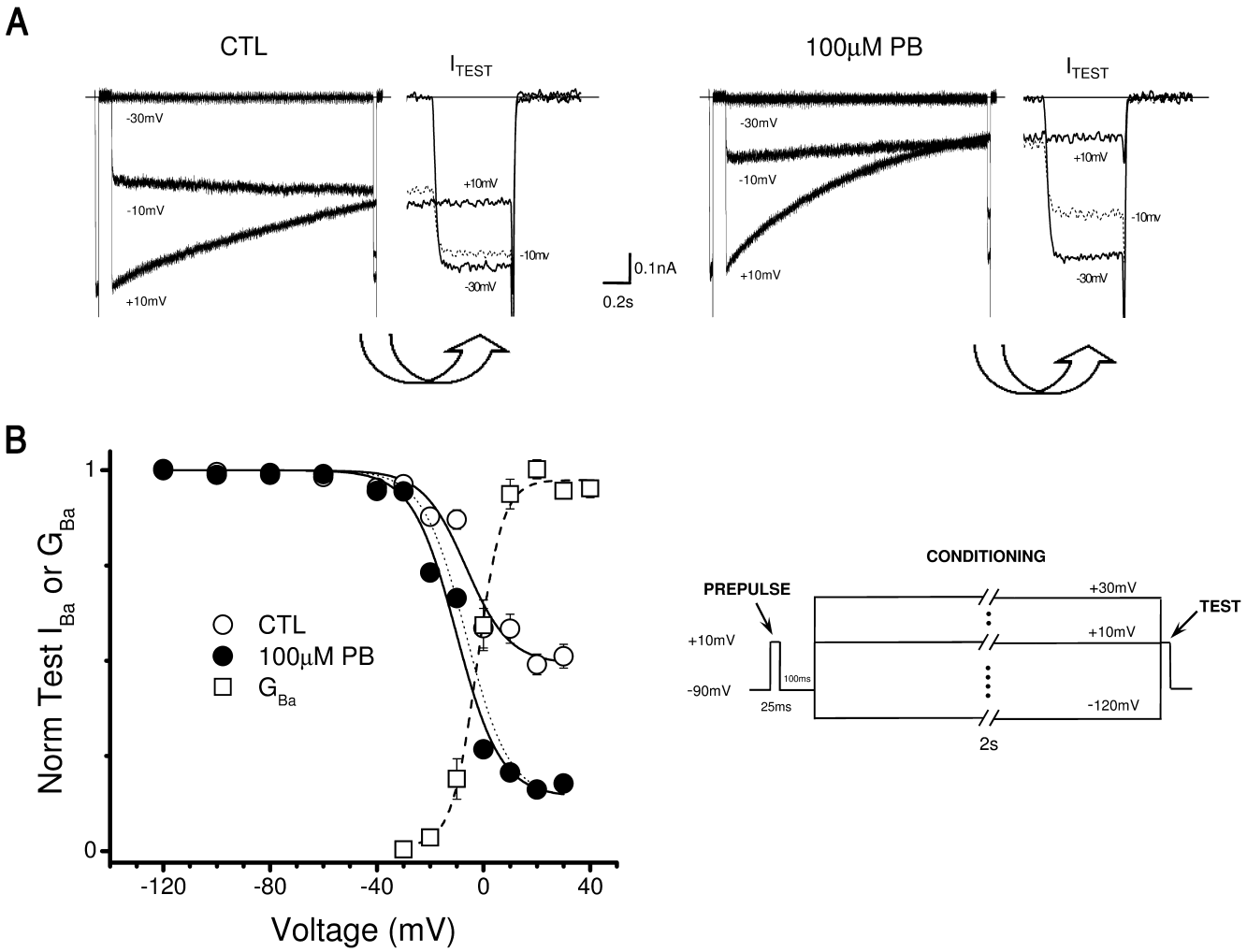

Figure 4

Voltage dependence of channel availability. (A) Selected I_{Ba} responses triggered by conditioning pulse voltages indicated in control (CTL, left) and pentobarbital (PB, right) from a cell expressing PQCCs, using the voltage protocol described in (B, inset). Test pulse current (I_{TEST}) displayed on expanded time scale for clarity as indicated by curved arrows. (B) the amplitude of I_{TEST} normalized to that of the pre-pulse current and plotted versus conditioning pulse voltage for control and PB in grouped data (means ± SEM, $n = 3–9$). These relationships show the voltage dependence of channel availability and represent non-steady-state inactivation curves. Solid smooth lines are Boltzmann fits of control and PB relationships (CTL: $V_{1/2} = -7.1 \pm 2.1$ mV, $dx = 8.0 \pm 2$, $P = 0.49 \pm 0.03$; PB: $V_{1/2} = -10.1 \pm 1.9$ mV, $dx = 8.3 \pm 1.4$, $P = 0.14 \pm 0.03$; estimated parameter value ± SE). Boltzmann fit of CTL normalized to that of PB (dotted line) illustrates the similar shape of these relationships. Normalized conductance in Ba^{2+} (G_{Ba}) and associated Boltzman function fit (dashed curve) were replotted from Figure 2C. PB effects on voltage-dependent inactivation occurred over a voltage range where channels activate, suggesting that channels states near opening are targeted by PB.

PB depressed channel availability by deepening non-steady-state inactivation

To further explore the role of VDI in the PB action, we examined the dependence of channel availability on HP using a three pulse inactivation protocol (Figure 4B, inset). Figure 4A (left) shows selected I_{Ba}s from an individual cell in control. Conditioning pulse voltages greater than –30 mV triggered currents and reduced channel availability as reported by the amplitude of the test pulse I_{Ba}. Grouped data support this finding (Figure 4B) where only voltages greater than –30 mV reduced channel availability. Increasing depolarization produced progressive decreases in channel availability, reaching a non-zero plateau near +20 mV, therefore representing a non-steady-state inactivation curve. The voltage range which reduced channel availability (–20 to +20 mV) coincided with that for channel activation and accords with a gating mechanism in which open, and not resting, states undergo VDI. This accords with previous reports in PQCCs with the β_{2a} accessory subunit (Patil *et al.*, 1998) and indicates classical open-state inactivation (Armstrong and Bezanilla, 1977; Bean,

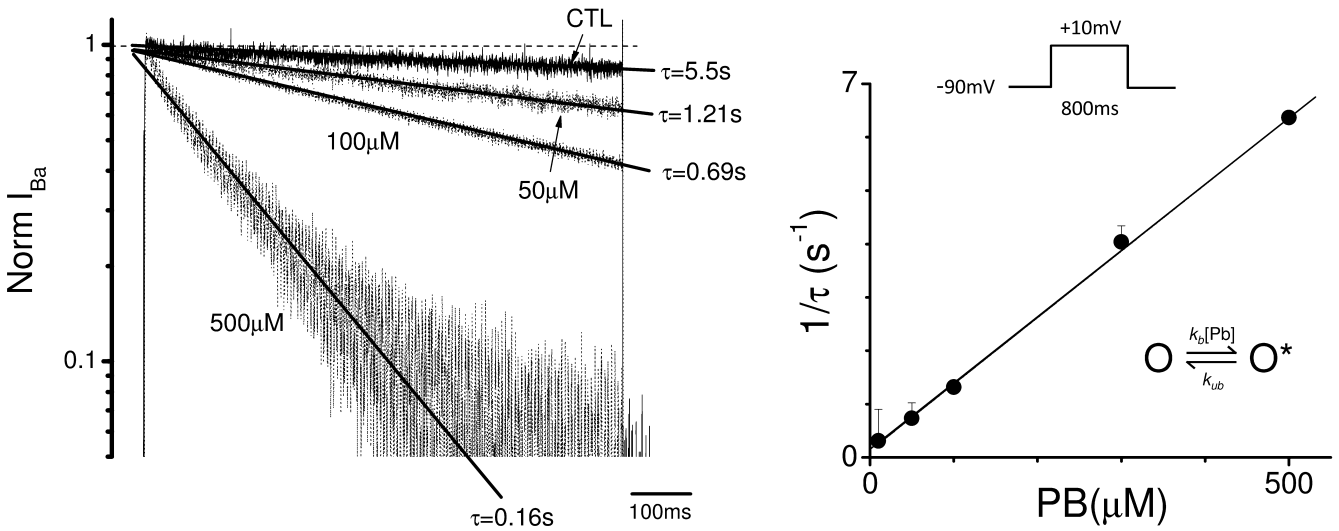

Figure 5

Concentration dependence of pentobarbital-induced acceleration of I_{Ba} decay. (*A*) Semi-logarithmic plots of I_{Ba}s triggered by 800 ms test pulses (protocol, right panel above inset) at indicated PB concentration from individual cells expressing PQCCs. The decay time course was well fit by a mono-exponential function (straight lines) for each response and is labelled with the corresponding time constant (τ). Mono-exponential functions appear linear on these axes. (*B*) Plot of 1/τ versus PB concentration (means ± SEM, n = 3–6) shows a linear relationship (slope = 12.2[s × PB (mM)]$^{-1}$, intercept = 0.2 s^{-1}). Lower inset shows simple open channel blocking scheme where open channels (O) become blocked (O*) which is governed by a bimolecular binding reaction in which the blocking rate is the product of the blocking rate constant (k_b) and PB concentration ([PB]) and the unblock rate (k_{ub}). Upper inset shows voltage protocol, stimulus period of 60 s.

1981) without appreciable preferential closed-state inactivation.

PB 100 μM potentiated the fraction of unavailable channels over the same voltage range as in control for individual cell responses and in grouped data (Figure 4A,B). Both control and PB inactivation curves were well fit (see Methods) by two state Boltzmann relationships with similar midpoint and slopes (control, $V_{1/2}$ = –7.1 ± 2.1 mV; dx = 8.0 ± 2; P = 0.49 ± 0.03; PB, $V_{1/2}$ = –10.1 ± 1.7 mV, dx = 8.28 ± 1.4, P = 0.14 ± 0.04; estimated parameter value ± SE). Therefore, PB deepened the inactivation curve without a voltage shift or change in slope, which is visually demonstrated by the similarity of the PB inactivation curve to that of the scaled control response (dotted line). The results point to two conclusions. First, transitions from resting closed to inactivated states are unlikely to underlie peak current depression. Second, PB acts on states associated with activation, open or inactivated, by a mechanism that involves either PB block of open channels or promotion of VDI states.

PB accelerated current decay consistent with slow, open channel block

To distinguish between mechanisms of VDI enhancement and open channel block, we analysed the effects of PB on the time course of I_{Ba} over a range of PB concentrations. The kinetic nature of I_{Ba}s was revealed using semilogarithmic plotting, which transforms exponential components into linear phases. Figure 5 (left) shows that current responses in PB are composed primarily of a single exponential component with a time constant that is progressively reduced with increasing PB concentration. Plotting the reciprocal time constants, equal to associated rates, versus PB concentration (Figure 5, right) yielded a linear relationship. These findings can be parsimoniously accounted for by a mechanism involving a bimolecular binding with a single binding site that, when occupied, blocks the open state. In this analysis, the slope describes the blocking rate constant (k_b) and the ordinate intercept marks the unblocking rate (k_{ub}). The fitted parameters (k_b = 12.2[s × PB (mM)]$^{-1}$, k_{ub} = 0.2 s^{-1}) indicate that this is a slow binding reaction (computed K_d = 15 μM). The results indicate a simple open channel blocking mechanism involving bimolecular binding. However, a more complex mechanism involving allosteric modulation of VDI cannot be excluded.

PB increased unavailable channel states and slowed recovery

Recovery from activity-induced, unavailable states was examined using a three pulse protocol (Figure 6B, right). Control responses from an individual cell (Figure 6A, left) showed that a condition-

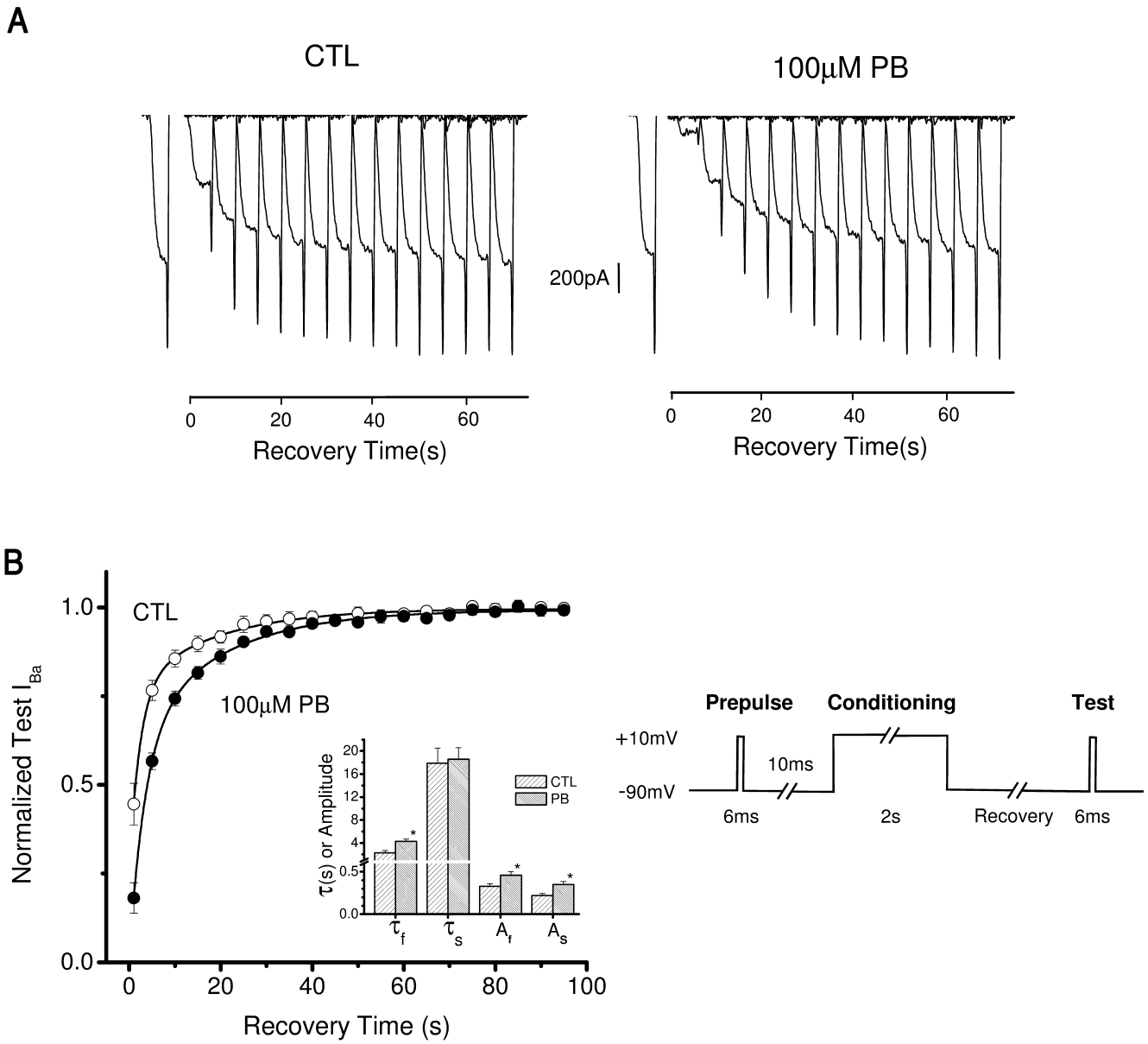

Figure 6

I_{Ba} recovery from voltage-dependent inactivation and pentobarbital (PB) block. (*A*) I_{Ba} recovery families triggered by indicated voltage protocol (*B*, right) used to assess recovery (at 1 s and 5 s, then at 5 s intervals thereafter) from an inactivating conditioning pulse (+10 mv) in control (CTL, left) and 100 μM pentobarbital (PB, right) from individual cells expressing P/Q-type voltage-gated Ca^{2+} channels. (*B*) Peak test pulse I_{Ba} normalized to that of the pre-pulse current plotted versus time after conditioning pulse end (recovery time) with bi-exponential curve fits (curved solid lines) in CTL and 100 μM PB (means ± SEM, $n = 5$). Left, inset, histogram showing the fast and slow time constants (τ_{fast} and τ_{slow}) and amplitudes (A_{fast} and A_{slow}) for bi-exponential function fits (estimated parameter value ± SE) of recovery responses (see Methods). Asterisks indicate statistically significant differences between control and PB ($P < 0.05$).

ing (2 s) pulse rendered about 60% of channels unavailable, as revealed by the first test pulse I_{Ba} amplitude relative to that of the pre-pulse presumably due to VDI. Later, test pulses triggered I_{Ba}s that charted a recovery time course that appeared to be biphasic in nature and where recovery was complete in approximately 60 s. PB 100 μM drove a greater fraction of channels into unavailable states (>80%) and appeared to slow the recovery time course. These observations in individual cells were confirmed in grouped data (Figure 6B). The control recovery time course was well fit (see Methods) by a bi-exponential function with fast and slow components where the fast component ($\tau_f \approx 3$ s) was dominant (Figure 6B, inset). These findings are consistent with previous results (Lee *et al.*, 2000). PB increased

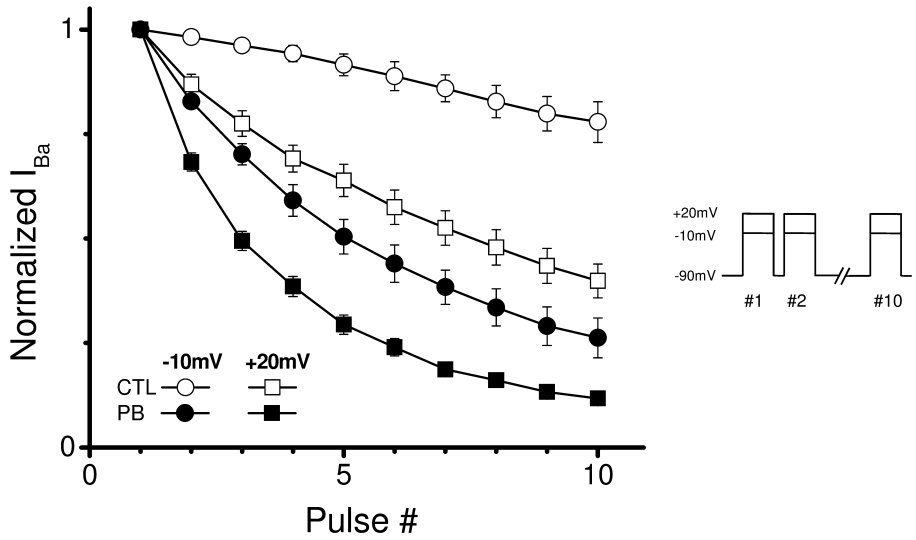

Figure 7

Use-dependent block by pentobarbital (PB) in low-frequency pulse trains. Plots of peak I_{Ba} normalized to the peak of the first pulse current triggered by repetitive low-frequency (2 Hz) step depolarizations (400 ms) to –10 mV and +20 mV according to the indicated protocol (means ± SEM, n = 3–4). The decrease of the I_{Ba} over the train of pulses represents an accumulation of inactivated channels in control. The enhanced reduction of this current in the presence of PB represents use-dependent block, see text.

the fraction of unavailable channels by promoting both fast and slow components but slowed overall recovery primarily by increasing the magnitude (A_f) and time constant (τ_f) of the fast component (Figure 6B, inset).

PB produced use-dependent block

The dual PB effects of increasing activity-induced channel unavailability and slowing recovery from these states may give rise to use-dependent block. Use-dependent block occurs with repetitive stimulation in which the time between stimuli is insufficiently long to allow recovery of drug- and activity-induced unavailable states leading to their accumulation and incremental depression of subsequent currents (Courtney, 1975). We tested for simple use-dependent block by PB using a pulse train protocol (Figure 7, inset). In control, the pulse train (–10 mV) produced a small decrease in the current consistent with minor accumulation of VDI states. PB (100 μM) produced a marked use-dependent block in which more than 70% of channels were unavailable at the end of the pulse train. More depolarized potentials (+20 mV) caused enhancement of inactivation leading to significant accumulation of VDI states and marked reduction of available states in control. PB also produced use-dependent block over this pulse train as well, but fractionally less than with –10 mV depolarizations since channel availability was markedly reduced in control.

PB induced use-dependent block of high frequency, physiological pulse trains

PB use-dependent block (Figure 7) prompted us to consider whether use-dependent block is also manifest during physiological, high frequency stimuli. Therefore, we examined the effects of a clinically relevant PB concentration (100 μM) on I_{Ca}s elicited by 200 Hz trains of 2 ms depolarizations (Figure 8A, inset), which roughly approximates neuronal action potential waveforms (Penington *et al.*, 1992; Toth and Miller, 1995) and frequencies observed in the mammalian CNS (Ylinen *et al.*, 1995). Tail current amplitudes (I_{Tail}) were taken as an indication of channel activation since peak I_{Ca} was difficult to determine when triggered by brief 2 ms pulses (see Figure 8A, exploded inset). In control, I_{Tail}s from an individual cell initially increased by approximately 25% within the first 100 ms of the pulse train (Figure 8A), reflecting CDF. This degree of facilitation is similar to that observed pre-synaptically (Borst *et al.*, 1995) and in other reports with recombinant PQCCs (Lee *et al.*, 2000; Chaudhuri *et al.* 2007). Subsequently, I_{Tail} amplitudes progressively declined throughout the remainder of the pulse train representing accumulation of inactivated states. PB depressed the first I_{Tail} consistent with resting block. PB appeared to attenuate early I_{Tail} potentiation by CDF and accelerate the decrease of I_{Tail} following the peak presumably due to use-dependent blockade. These observations were confirmed in grouped data (Figure 8B, left). The peak

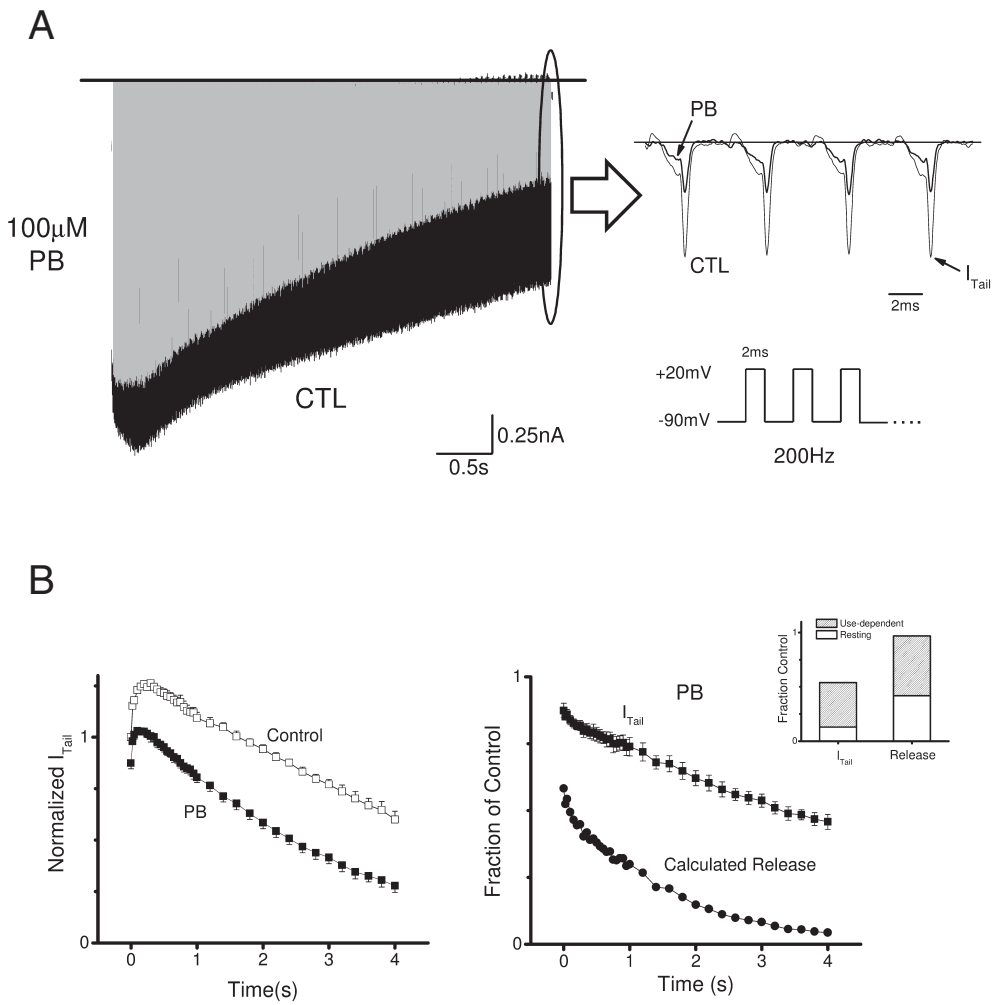

Figure 8

Inhibition of peak I_{Ca} in physiological high-frequency pulse trains. (A) I_{Ca} families (left) triggered by pulse trains (inset, below) from an individual cell expressing P/Q-type voltage-gated Ca^{2+} channels in control (CTL) and 100 μM pentobarbital (PB) as indicated. The boundaries or envelopes of the current families are formed by tail currents that are reflective of peak I_{Ca} and channel activation during the triggering pulse. Upper inset, ellipse encircles portion of pulse trains that are replotted on expanded timescale to illustrate differences in the I_{Ca} time course in CTL and PB. Peak tail current (I_{Tail}) was taken as an indication of peak channel activation. (*B*) Left, I_{Tail} amplitude normalized to that of the first I_{Tail} in control and plotted versus pulse train duration (means ± SEM, $n = 3$) in CTL and PB. Every 10th (every 50 ms) response was evaluated in the first second and every 40th response (every 200 ms) for the remainder of the pulse train (3 s). The control response increased initially due to CDF, reached a peak, and then decayed. PB depressed channel activation over the entire pulse train. (*B*) Right, plot of normalized PB I_{Tail} and calculated synaptic release (calculated release) as a fraction of control. The calculated release was computed as the 4th power of the I_{Tail} response. Inset, plot of the contributions of resting and use-dependent block to the pulse train, both as a fraction of control, during the PB-mediated depression of I_{Tail} and calculated release.

I_{Tail} response relationship normalized to that of control (Figure 8B, right) indicates that PB inhibition was more than twofold over the pulse train. Neurotransmitter release varies with pre-synaptic Ca^{2+} influx by a power function of up to 4 (Dodge and Rahamimoff, 1967; Katz and Miledi, 1970; Augustine *et al.*, 1987; Zucker and Regehr, 2002). Therefore, to explore the potential effects of PB PQCC inhibition on synaptic transmission, we computed neurotransmitter release (calculated release) as a 4^{th}-order function of channel activation (normalized I_{Tail}) (Figure 8B). The relationship shows that resting block inhibited calculated release with the first pulse by nearly 40%. Use-dependent block presumably suppressed calculated release further by >60% over the next 150 ms, which reached >90% by the end of the pulse train. Relative contributions of resting and use-dependent block to depression of I_{Tail} and calculated release over the course of the pulse train show that both contribute significantly where use-dependent block is predominant (Figure 8B, inset). The results suggest that PB, at

clinical concentrations, may produce significant synaptic depression particularly during high frequency PQCC activation.

Discussion and conclusions

Mechanism of PB block

PB inhibited I_{peak} in a concentration-dependent manner (Figure 1) which may be accounted for by block of resting channels, altered activation, rapid open channel block or transitions from resting to inactivated states. PB depressed I_{peak} without altering the voltage dependence of activation (Figure 2) arguing against altered activation. The kinetics of open channel block are more than hundred-fold slower than those of activation, discounting a significant contribution to peak current depression (Figure 5). PB deepened non-steady-state inactivation curves without changes in midpoint ($V_{1/2}$) and slope (dx) of Boltzmann function fits (Figure 4) which argues against transitions from resting or nearby closed states to inactivated states prior to opening, thereby supporting resting channel block. Furthermore, channel availability reported by non-steady-state inactivation curves decreased over a voltage range, which also triggers activation, consistent with open or nearby channel states undergoing block or enhanced inactivation. Taken together, these findings indicate strongly that PB blocks resting channels and that this underlies I_{peak} inhibition. Insight into the underlying binding reaction can be derived from the I_{peak} inhibition relationship assuming that it primarily reflects binding. The fitted logistic function to this relationship (Figure 1) yielded an IC_{50} of ~600 μM and a slope factor of ~0.8 pointing to bimolecular binding with a K_d of 600 μM.

PB accelerated current decay reported by r_{800} in a concentration-dependent fashion independent of charge carrier (Figure 1), which discounts a role of CDI. Current decay was enhanced by depolarization that reached a maximum near the plateau of the G–V relationship (Figure 3) and maximal peak open probability. PB decreased channel availability reported by non-steady-state inactivation curves over a voltage range that triggered activation (Figure 4). Overall, the results can be explained by either block of open or nearby channel states or, alternatively, enhanced VDI. To discriminate between these possibilities, we examined the nature of the PB-induced acceleration of mono-exponential current decay and found that associated rates were linearly dependent on PB concentration (Figure 5). PB also increased the fraction of activity-induced unavailable states and slowed their recovery primarily by increasing the magnitude and time constant of the fast component of a bi-exponential recovery time course (Figure 6). These findings may arise from a novel drug-bound blocked state with recovery kinetics slower but similar to that of the fast component in control, thereby rendering them kinetically un-resolvable. Alternatively, it may be explained by drug-induced slowing of recovery from fast inactivated states. Overall, these results lead us to a conclusion of open channel block, but a more complex mechanism involving allosteric modulation of VDI cannot be excluded.

The proposed mechanism of open channel block may involve an intrapore receptor that, when occupied, occludes the permeation pathway and renders the channel non-conducting. The concentration dependence of current decay rate (Figure 5) suggests that the underlying binding is bimolecular (K_d = 15 μM), and kinetically slow. The apparent macroscopic kinetics of the presumed open channel block are slow with time constants in the order of fractional seconds. Simple open channel block that is manifest in macroscopic currents is determined by the underlying microscopic binding reaction and the open state probability. The open state probability of PQCCs is low (Sather *et al*., 1993; Chaudhuri *et al*. 2007) and reported to be <0.05 with Ba^{2+} as the charge carrier (+20 mV) (Chaudhuri *et al*., 2007). Therefore, microscopic binding rates may be more than an order of magnitude greater than those inferred from macroscopic currents. Overall, the findings support a modulated receptor mechanism, where the binding affinity (K_d = 15 μM) of open channel block is 40-fold greater than for resting block.

Comparison with previous studies of PB and neuronal VACCs

Nishi and Oyama (1983) studied VACCs in *Helix* F-1 neurones and found that barbiturates (thiopentone, PB and phenobarbitone) depressed peak current without shifting the current–voltage relationship, accelerated apparent inactivation and leftward shifted a two-pulse inactivation curve. The authors concluded that barbiturates, including PB, produced inhibition by enhancing VDI. Similar results have been reported by Gundersen *et al*. (1988) in ω-conotoxin-sensitive, dihydropyridine-resistant VACCs, thereby probably N-type ($Ca_V2.2$), obtained from the expression of human temporal lobe mRNA in *Xenopus*; by Gross and Macdonald (1988) for N-type currents in mouse dorsal root ganglia; and by Ikemoto *et al*. (1986) in *Aplysia* neurones. A leftward shift of the inactivation curve is a key finding in support of barbiturate enhancement of VDI. In contrast, we found that PB failed to shift the inactiva-

tion curve of PQCCs in accord with an open channel blocking mechanism. This discrepancy may be due to preparation differences or reflect distinct barbiturate pharmacology between PQCCs and $Ca_V2.2$ channels, as reported for other VACCs (Gross and Macdonald, 1988).

Ffrench-Mullen *et al*. (1993) investigated the effects of barbiturates (phenobarbital, 5-(2-cyclohexylideneethyl)-5-ethyl barbituric acid, PB and its optical entantiomers: R(–)-PB, S(+)-PB) on a mixed population of VACCs from hippocampal CA1 cells. The IC_{50}s for the optical entantiomers, R(–)-PB and S(+)-PB, were 3.5 μM and >1000 μM, respectively, indicating stereospecific inhibition. R(–)-PB blocked peak current in a voltage-dependent fashion sensing 40% of the membrane electric field from the extracellular surface, was pH dependent and accelerated a slow component of bi-exponential inactivation. Voltage-dependent inhibition of peak current contrasts with the results of this and earlier studies (Nishi and Oyama, 1983;Gundersen *et al*., 1988). We were interested in investigating the effects of optical enantiomers of PB in our preparation but were unable to acquire the molecules.

There is only one investigation, to our knowledge, that has selectively examined PB modulation of PQCCs (Hall *et al*., 1994). The authors reported little reduction (6.4%) of peak I_{Ba} by 50 μM PB in *ex vivo* rat cerebellar Purkinje cells and the investigation did not address inactivation. Acknowledging that PB anaesthetic potency is greater in human than in rat (Spector, 1956; Franks and Lieb, 1994), we explored PB action on PQCCs with a human primary α_{1A} subunit to begin to investigate the possible underpinnings of this species difference. We found in this study a nearly twofold greater reduction (11%) in peak I_{Ba}. The discrepancies in peak current blocking potency of PB between these studies may be due to preparation differences, but may also reflect genuine species-dependent pharmacological phenotypes since α_{1A} peptide homology differs by ~10% between rat and human (Zhuchenko *et al*., 1997). Whether this variation in protein structure of the α_1 subunit of PQCCs underlies the differences in PB potency awaits future structure-function analysis.

Pharmacology of other PQCC inhibitors

PQCCs are inhibited by the peptide toxins *Agelenopsis aperta* spider ω-agatoxin-IVA (Mintz *et al*., 1992), and marine cone snail *Conus magus* ω-conotoxin-MVIIC (Hillyard *et al*., 1992), which are irreversible blockers (Olivera *et al*., 1994; Garcia-Palomero *et al*. 2000). SNX482, isolated from the venom of an African tarantula, *Hysteocrates gigas*, produces reversible inhibition of PQCCs (Arroyo *et al*., 2003). Small organic blocking molecules include antazoline (Milhaud *et al*., 2002), and the benzimidazolyl-substituted tetraline derivative, mibefradil (Fang and Osterrieder, 1991; Bezprozvanny and Tsien, 1995; Aczel *et al*., 1998). Mibefradil has been the most extensively investigated and its inhibition of PQCC involves accelerated apparent inactivation with (Fang and Osterrieder, 1991; Bezprozvanny and Tsien, 1995) or without (Aczel *et al*., 1998) leftward shifting of the inactivation curve leading to proposed mechanisms of either enhanced VDI or open channel blockade, respectively. Aczel *et al*. (1998) also reported use-dependent block with this drug, slowed recovery from activity-induced unavailable channels and slow drug-induced current decay occurring over fractions of seconds (Figure 3A, Aczel *et al*., 1998)). These results are remarkably similar to those of PB inhibition of PQCCs in this study. Mibefredil is highly lipophilic with titratable hydrogen ion sites at a benzimidazolyl group (pK_a = 4.8) and the tertiary amine (pK_a = 5.5). PB is also highly lipophilic and, like other barbiturates, the ring nitrogens can shed a hydrogen ion (pK_a = 8.0) through resonance stabilization by a flanking carbonyl group leading to an anionic molecule. Given this acid-base chemistry, both molecules are largely uncharged at physiological pH and remain lipophilic. The similarities between these two organic molecules at inhibiting PQCCs make it interesting to speculate that both may share a pharmacological mechanism involving preferential binding of the neutral drug form to a lipophilic binding pocket of open channels culminating in blockade. This speculation awaits identification of binding sites mediating PQCC inhibition for each of these drugs.

PB effects on pre-synaptic neurotransmitter release

We are aware of two reports addressing PB modulation of pre-synaptic neurotransmitter release. Kitayama *et al*. (2002) investigated the effects of PB and other anaesthetic agents on K^+-evoked glutamate release from rat cerebrocortical slices and found that glutamate release was completely blocked by selective inhibitors of PQCCs, and potently inhibited by PB (50% inhibitory concentration: 8.3 μM). The authors concluded that inhibition of glutamate release by clinical concentrations of PB is mainly due to direct PQCC inhibition, although a role of $GABA_A$ receptor activation could not be excluded. Baudoux *et al*. (2003) studied excitatory post-synaptic potentials (EPSP) and Ca^{2+} transients in axonal varicosities and fine axon collaterals of hippocampal CA1 neurones. PB (150 μM) depressed Ca^{2+} transients recorded from

synaptic boutons and reduced the amplitude and frequency of spontaneous EPSPs. The authors proposed that PB inhibition of pre-synaptic Ca^{2+} transients contributes to its depressant effect on excitatory synaptic transmission in the CNS. Overall, the above results are consistent with the notion that PB inhibits pre-synaptic Ca^{2+} influx leading to reduced release of neurotransmitter and synaptic depression.

Possible clinical relevance of PB inhibition of PQCCs

The range of free PB concentrations that produce anticonvulsant activity in man is 50–100 μM (Raines *et al*. 1979; Heyer and Macdonald, 1982), and for anaesthesia, the range is slightly higher at 50–150 μM (Richards, 1972; Heyer and Macdonald, 1982; Franks and Lieb, 1994). PB resting block depressed peak current by 16% at clinically relevant concentrations (100 μM), which is similar in absolute magnitude to the effects of CDF, G-protein modulation and intrinsic inactivation, all of which play critical roles in PQCC modulation of underlying synaptic plasticity (Catterall, 2000; Tedford and Zamponi, 2006). The magnitude of this effect corresponds to a nearly twofold reduction in computed neurotransmitter release, assuming a fourth-order relationship between peak Ca^{2+} entry and release (Dodge and Rahamimoff, 1967; Katz and Miledi, 1970; Augustine *et al*., 1987; Zucker and Regehr, 2002). Additional PQCC depression may occur with high frequency repetitive stimulation sufficient to induce use-dependent block. We observed use-dependent block during physiological high frequency (200 Hz) pulse trains which, when combined with resting block, produced overall PQCC inhibition of 21, 25, 32 and 49% at 150, 500, 1000 and 3000 ms time points during the pulse train, respectively (Figure 8). These produced corresponding depressions of computed synaptic release of 61, 68, 79 and 93%, respectively. Therefore, volleys of high frequency action potential trains may cause further synaptic depression through use-dependent block of PQCCs. The relevance of use-dependent block to anaesthetic action is supported by reports of firing frequencies in the mammalian CNS of up to 200 Hz (Ylinen *et al*., 1995). Epileptogenic foci in the cortex and CA3 hippocampal region fire high-frequency bursts of action potentials with frequencies reaching 500 Hz (Ward, 1969; Calvin, 1972). These higher firing frequencies would presumably induce greater use-dependent block and synaptic depression in the associated local neural circuit, thereby extinguishing the CNS dysrhymthia before it is able to generalize. Use-dependent block plays a critical role in the inhibition of voltage-gated channels by some clinical anticonvulsants (Ragsdale and Avoli, 1998) and cardiac antidysrhythmics (Rosen and Wit, 1983), but is less common in the clinical utility of inhibitors of neuronal VACCs. The findings are consistent with the hypothesis that PQCC inhibition contributes to the CNS depression produced by PB during general anaesthesia and anticonvulsant therapy.

PQCCs are generally thought to play a dominant role in neurotransmitter release at most fast synapses in the mammalian CNS (Catterall and Few, 2008), which include both excitatory and inhibitory connections. However, at some hippocampal synapses, release of the inhibitory neurotransmitter γ-aminobutyric acid is governed predominantly by $Ca_V2.2$ channels (N-type currents) (Poncer *et al*., 1997; 2000). Overall, the contribution of PB-induced inhibition of PQCCs to clinical anaesthesia and anticonvulsant therapy remains an open question and awaits elucidation of critical neuronal circuits modulated to produce the clinical effect.

Acknowledgements

This study was supported by a Foundation for Anesthesia Education and Research grant to A S and by the NYU Langone Medical Center, Department of Anesthesiology Research Fund.

Statement of conflicts of interest

None.

References

Aczel S, Kurka B, Hering S (1998). Mechanism of voltage- and use-dependent block of class A Ca^{2+} channels by mibefradil. Br J Pharmacol 125: 447–454.

Alexander SP, Mathie A, Peters JA (2008). Guide to Receptors and Channels (GRAC), 3rd Edition. Br J Pharmacol 153 (Suppl. 2): S1–S209.

Armstrong CM, Bezanilla F (1977). Inactivation of the sodium channel. II. Gating current experiments. J Gen Physiol 70: 567–590.

Arroyo G, Aldea M, Fuentealba J, Albillos A, Garcia AG (2003). SNX482 selectively blocks P/Q Ca^{2+} channels and delays the inactivation of Na+ channels of chromaffin cells. Eur J Pharmacol 475: 11–18.

Augustine GJ, Charlton MP, Smith SJ (1987). Calcium action in synaptic transmitter release. Annu Rev Neurosci 10: 633–693.

Baudoux S, Empson RM, Richards CD (2003). Pentobarbitone modulates calcium transients in axons and synaptic boutons of hippocampal CA1 neurons. Br J Pharmacol 140: 971–979.

Bean BP (1981). Sodium channel inactivation in the crayfish giant axon. Must channels open before inactivating? Biophys J 35: 595–614.

Bezprozvanny I, Tsien RW (1995). Voltage-dependent blockade of diverse types of voltage-gated Ca^{2+} channels expressed in *Xenopus* oocytes by the Ca^{2+} channel antagonist mibefradil (Ro 40-5967). Mol Pharmacol 48: 540–549.

Borst JG, Helmchen F, Sakmann B (1995). Pre- and postsynaptic whole-cell recordings in the medial nucleus of the trapezoid body of the rat. J Physiol 489 (Pt 3): 825–840.

Brooks CM, Eckert R (1947). A study of the effect of anesthesia on the monosynaptic pathway of the spinal cord. J Neurophysiol 10: 340–360.

Calvin WH (1972). Synaptic potential summation and repetitive firing mechanisms: input–output theory for the recruitment of neurons into epileptic bursting firing patterns. Brain Res 39: 71–94.

Catterall WA (2000). Structure and regulation of voltage-gated Ca^{2+} channels. Annu Rev Cell Dev Biol 16: 521–555.

Catterall WA, Few AP (2008). Calcium channel regulation and presynaptic plasticity. Neuron 59: 882–901.

Catterall WA, Striessnig J, Snutch TP, Perez-Reyes E (2003). International union of pharmacology. XL. Compendium of voltage-gated ion channels: calcium channels. Pharmacol Rev 55: 579–581.

Chao SH, Suzuki Y, Zysk JR, Cheung WY (1984). Activation of calmodulin by various metal cations as a function of ionic radius. Mol Pharmacol 26: 75–82.

Chaudhuri D, Issa JB, Yue DT (2007). Elementary mechanisms producing facilitation of $Ca_v^{2.1}$ (P/Q-Type) channels. J Gen Physiol 129: 385–401.

Courtney KR (1975). Mechanism of frequency-dependent inhibition of sodium currents in frog myelinated nerve by the lidocaine derivative GEA. J Pharmacol Exp Ther 195: 225–236.

DeMaria CD, Soong TW, Alseikhan BA, Alvania RS, Yue DT (2001). Calmodulin bifurcates the local Ca^{2+} signal that modulates P/Q-type Ca^{2+} channels. Nature 411: 484–489.

Dodge FA Jr, Rahamimoff R (1967). Co-operative action a calcium ions in transmitter release at the neuromuscular junction. J Physiol 193: 419–432.

Erickson MG, Alseikhan BA, Peterson BZ, Yue DT (2001). Preassociation of calmodulin with voltage-gated Ca(2+) channels revealed by FRET in single living cells. Neuron 31: 973–985.

Evans RH (1979). Potentiation of the effects of GABA by pentobarbitone. Brain Res 171: 113–120.

Fang LM, Osterrieder W (1991). Potential-dependent inhibition of cardiac Ca2+ inward currents by Ro 40-5967 and verapamil: relation to negative inotropy. Eur J Pharmacol 196: 205–207.

ffrench-Mullen JM, Barker JL, Rogawski MA (1993). Calcium current block by (-)-pentobarbital, phenobarbital, and CHEB but not (+)-pentobarbital in acutely isolated hippocampal CA1 neurons: comparison with effects on GABA-activated Cl- current. J Neurosci 13: 3211–3221.

Franks NP, Lieb WR (1993). Selective actions of volatile general anaesthetics at molecular and cellular levels. Br J Anaesth 71: 65–76.

Franks NP, Lieb WR (1994). Molecular and cellular mechanisms of general anaesthesia. [Review] [129 Refs]. Nature 367: 607–614.

Garcia-Palomero E, Montiel C, Herrero CJ, Garcia AG, Alvarez RM, Arnalich FM *et al.* (2000). Multiple calcium pathways induce the expression of SNAP-25 protein in chromaffin cells. J Neurochem 74: 1049–1058.

Gingrich KJ, Burkat PM, Roberts WA (2009). Pentobarbital produces activation and block of $\alpha1\beta2\gamma2S$ GABA-A receptors in rapidly perfused whole cells and membrane patches: divergent results can be explained by pharmacokinetics. J Gen Physiol 133: 171–188.

Gross RA, Macdonald RL (1988). Differential actions of pentobarbitone on calcium current components of mouse sensory neurones in culture. J Physiol 405: 187–203.

Gundersen CB, Umbach JA, Swartz BE (1988). Barbiturates depress currents through human brain calcium channels studied in *Xenopus* oocytes. J Pharmacol Exp Ther 247: 824–829.

Hall AC, Lieb WR, Franks NP (1994). Insensitivity of P-type calcium channels to inhalational and intravenous general anesthetics. Anesthesiology 81: 117–123.

Heyer EJ, Macdonald RL (1982). Barbiturate reduction of calcium-dependent action potentials: correlation with anesthetic action. Brain Res 236: 157–171.

Hillyard DR, Monje VD, Mintz IM, Bean BP, Nadasdi L, Ramachandran J *et al.* (1992). A new conus peptide ligand for mammalian presynaptic Ca2+ channels. Neuron 9: 69–77.

Ikemoto Y, Mitsuiye T, Ishizuka S (1986). Reduction of the voltage-dependent calcium current in aplysia neurons by pentobarbital. Cell Mol Neurobiol 6: 293–305.

Joksovic PM, Brimelow BC, Murbartian J, Perez-Reyes E, Todorovic SM (2005). Contrasting anesthetic sensitivities of T-type Ca2+ channels of reticular thalamic neurons and recombinant Ca(v)3.3 channels. Br J Pharmacol 144: 59–70.

Katz B, Miledi R (1970). Further study of the role of calcium in synaptic transmission. J Physiol 207: 789–801.

Kitayama M, Hirota K, Kudo M, Kudo T, Ishihara H, Matsuki A (2002). Inhibitory effects of intravenous anaesthetic agents on K(+)-evoked glutamate release from rat cerebrocortical slices, involvement of voltage-sensitive Ca(2+) channels and GABA(A) receptors. Naunyn Schmiedebergs Arch Pharmacol 366: 246–253.

Lee A, Scheuer T, Catterall WA (2000). Ca2+/calmodulin-dependent facilitation and inactivation of P/Q-type Ca2+ channels. J Neurosci 20: 6830–6838.

Lee A, Wong ST, Gallagher D, Li B, Storm DR, Scheuer T *et al*. (1999). Ca2+/calmodulin binds to and modulates P/Q-type calcium channels. Nature 399: 155–159.

Lee A, Zhou H, Scheuer T, Catterall WA (2003). Molecular determinants of Ca(2+)/calmodulin-dependent regulation of Ca(v)2.1 channels. Proc Natl Acad Sci U S A 100: 16059–16064.

Leslie SW, Friedman MB, Wilcox RE, Elrod SV (1980). Acute and chronic effects of barbiturates on depolarization-induced calcium influx into rat synaptosomes. Brain Res 185: 409–417.

Liang H, DeMaria CD, Erickson MG, Mori MX, Alseikhan BA, Yue DT (2003). Unified mechanisms of Ca^{2+} regulation across the Ca^{2+} channel family. Neuron 39: 951–960.

Macdonald RL, Rogers CJ, Twyman RE (1989). Barbiturate regulation of kinetic properties of the $GABA_A$ receptor channel of mouse spinal neurones in culture. J Physiology 417: 483–500.

Mathers DA, Barker JL (1980). (-)Pentobarbital opens ion channels of long duration in cultured mouse spinal neurons. Science 209: 507–509.

Milhaud D, Fagni L, Bockaert J, Lafon-Cazal M (2002). Inhibition of voltage-gated Ca^{2+} channels by antazoline. Neuroreport 13: 1711–1714.

Mintz IM, Venema VJ, Swiderek KM, Lee TD, Bean BP, Adams ME (1992). P-type calcium channels blocked by the spider toxin omega-aga-IVA. Nature 355: 827–829.

Morgan KG, Bryant SH (1977). Pentobarbital: presynaptic effect in the squid giant synapse. Experientia 33: 487–488.

Nishi K, Oyama Y (1983). Accelerating effects of pentobarbitone on the inactivation process of the calcium current in helix neurones. Br J Pharmacol 79: 645–654.

Olivera BM, Miljanich GP, Ramachandran J, Adams ME (1994). Calcium channel diversity and neurotransmitter release: the omega-conotoxins and omega-agatoxins. Annu Rev Biochem 63: 823–867.

Olsen RW (1988). Barbiturates. Int Anesthesiol Clin 26: 254–261.

Patil PG, Brody DL, Yue DT (1998). Preferential closed-state inactivation of neuronal calcium channels. Neuron 20: 1027–1038.

Penington NJ, Kelly JS, Fox AP (1992). Action potential waveforms reveal simultaneous changes in I_{Ca} and I_K produced by 5-HT in rat dorsal raphe neurons. Proc Biol Sci 248: 171–179.

Perez-Reyes E, Castellano A, Kim HS, Bertrand P, Baggstrom E, Lacerda AE *et al*. (1992). Cloning and expression of a cardiac/brain beta subunit of the L-type calcium channel. J Biol Chem 267: 1792–1797.

Poncer JC, McKinney RA, Gahwiler BH, Thompson SM (1997). Either N- or P-type calcium channels mediate GABA release at distinct hippocampal inhibitory synapses. Neuron 18: 463–472.

Poncer JC, McKinney RA, Gahwiler BH, Thompson SM (2000). Differential control of GABA release at synapses from distinct interneurons in rat hippocampus. J Physiol 528 (Pt 1): 123–130.

Ragsdale DS, Avoli M (1998). Sodium channels as molecular targets for antiepileptic drugs. Brain Res Brain Res Rev 26: 16–28.

Raines A, Blake GJ, Richardson B, Gilbert MB (1979). Differential selectivity of several barbiturates on experimental seizures and neurotoxicity in the mouse. Epilepsia 20: 105–113.

Richards CD (1972). On the mechanism of barbiturate anaesthesia. J Physiol 227: 749–767.

Rosen MR, Wit AL (1983). Electropharmacology of antiarrhythmic drugs. Am Heart J 106: 829–839.

Sather WA, Tanabe T, Zhang JF, Mori Y, Adams ME, Tsien RW (1993). Distinctive biophysical and pharmacological properties of class A (BI) calcium channel alpha 1 subunits. Neuron 11: 291–303.

Soong TW, DeMaria CD, Alvania RS, Zweifel LS, Liang MC, Mittman S *et al*. (2002). Systematic identification of splice variants in human P/Q-type channel Alpha1(2.1) subunits: implications for current density and Ca^{2+}-dependent inactivation. J Neurosci 22: 10142–10152.

Spector WS (1956). *Handbook of Biological Data*. W.B. Saunders: Philadelphia.

Stea A, Tomlinson WJ, Soong TW, Bourinet E, Dubel SJ, Vincent SR *et al*. (1994). Localization and functional properties of a rat brain alpha 1A calcium channel reflect similarities to neuronal Q- and P-type channels. Proc Natl Acad Sci U S A 91: 10576–10580.

Tanaka O, Sakagami H, Kondo H (1995). Localization of MRNAs of voltage-dependent Ca(2+)-channels: four subtypes of alpha 1- and beta-subunits in developing and mature rat brain. Brain Res Mol Brain Res 30: 1–16.

Tedford HW, Zamponi GW (2006). Direct G protein modulation of Ca_v^2 calcium channels. Pharmacol Rev 58: 837–862.

Todorovic SM, Perez-Reyes E, Lingle CJ (2000). Anticonvulsants but not general anesthetics have differential blocking effects on different T-type current variants. Mol Pharmacol 58: 98–108.

Tomlinson WJ, Stea A, Bourinet E, Charnet P, Nargeot J, Snutch TP (1993). Functional properties of a neuronal class C L-type calcium channel. Neuropharmacology 32: 1117–1126.

Toth PT, Miller RJ (1995). Calcium and sodium currents evoked by action potential waveforms in rat sympathetic neurones. J Physiol 485 (Pt 1): 43–57.

Ward AA (1969). Epileptic neuron: chronic foci in animals and man. In: Jasper HH, Ward AA, Pope A (eds). *Basic Mechanisms of the Epilepsies*. Little, Brown and Co: Boston, pp. 263–268.

Weakly JN (1969). Effect of barbiturates on 'quantal' synaptic transmission in spinal motoneurones. J Physiol 204: 63–77.

Ylinen A, Bragin A, Nadasdy Z, Jando G, Szabo I, Sik A *et al*. (1995). Sharp wave-associated high-frequency oscillation (200 Hz) in the intact hippocampus: network and intracellular mechanisms. J Neurosci 15: 30–46.

Zhuchenko O, Bailey J, Bonnen P, Ashizawa T, Stockton DW, Amos C *et al*. (1997). Autosomal dominant cerebellar ataxia (SCA6) associated with small polyglutamine expansions in the alpha 1A-voltage-dependent calcium channel. Nat Genet 15: 62–69.

Zucker RS, Regehr WG (2002). Short-term synaptic plasticity. Annu Rev Physiol 64: 355–405.